Research Square

Preprints are preliminary reports that have not undergone peer review.
They should not be considered conclusive, used to inform clinical practice,
or referenced by the media as validated information.

Structural-State Closure of the Full Stick–Slip Cycle: Reproducing the Inter-Slip Locked Phase and Delineating Its Boundary from Rate-and-State Friction

GuoJun Pan

18858146@qq.com

Independent Researche https://orcid.org/0009-0002-5750-6523

Research Article

Keywords: stick–slip friction; rate-and-state friction; structural state; acoustic emission; relax- ation spectrum; ice friction

Posted Date: November 9th, 2026

DOI: https://doi.org/10.21203/rs.3.rs-11646364/v1

License: This work is licensed under a Creative Commons Attribution 4.0 International License.
Read Full License

Additional Declarations: The authors declare no competing interests.

Structural-State Closure of the Full Stick–Slip Cycle: Reproducing the Inter-Slip Locked Phase and Delineating Its Boundary from Rate-and-State Friction

Guojun Pan
Independent Scholar, Qingdao, China
18858146@qq.com

October 30, 2026

Abstract

Statistical studies of stick–slip (the published PES companion [1]) describe the avalanche endpoint: event-size distributions, precursory signals, and critical slowdown. What remains unresolved is the *full time course*: during the long inter-slip (locked) loading period, how does the contact network of the frictional interface evolve continuously, and can a closed model reproduce the complete sequence and delimit its boundary against the continuous state-evolution equations of rate-and-state friction (RSF)? This paper develops a structural-state closure in which two unresolved interfacial coordinates carry the dynamics: a sliding-generated structure s (relaxing at a loading-rate-independent time $\tau_N = 1/b$), and a contact maturation m (Dieterich ageing). A high-speed liquid-lubrication floor closes the slip phase and renders the free block–spring self-sustaining. Three results follow. (i) *T1 exact reduction*: on the PES-validated speed branch the steady-state of the closure is identical to the published two-component ice-friction law of Pan [1] to a maximum deviation of 3.0×10^{-8}, and the free slider produces repeated stick–slip (153 events; mean recurrence 25.4; mean stress drop 0.302). (ii) *Locked-phase two-channel divergence*: during loading the structure softens (s relaxes) while maturation hardens (m ages), so the static strength is non-monotone (strength dip 0.071 at $t \simeq 19.9$), with slip nucleating near $t \simeq 688$. A single-state RSF law predicts monotone ageing only and cannot reproduce this dip. (iii) *Testable predictions*: (P2) the non-monotone dip of Dillavou and Rubinstein [5] is reproduced, but the experimental memory scaling $T_{\min} \propto T_W$ requires upgrading the structure channel to a power-law relaxation spectrum with logarithmic maturation — then the closure reproduces $T_{\min} = 0.59\,T_W$ against the AOI value $0.30\,T_W$; (P1) the precursory time span shortens with load-point velocity, consistent with the loading-rate series of Wang and Dresen [7]. We delineate the boundary: RSF performs well in monotone-aging and velocity-strengthening regimes, whereas the closure compensates for non-monotone recovery and memory scaling. All model results are reproducible from the enclosed reduced equations; experimental numbers are distinguished from model demonstrations throughout.

Keywords: stick–slip friction; rate-and-state friction; structural state; acoustic emission; relaxation spectrum; ice friction

1 Introduction

Frictional stick–slip is governed by a force balance between the loading-system stiffness and the critical stiffness of the interface [2–4]. Under a spring–slider paradigm, the slip mode (stable sliding versus unstable events) is fixed by the ratio of these stiffnesses, and repeated stick–slip arises when loading is slow and the interface restrengthens between events. Two broad questions motivate this work.

First, statistical studies of the *avalanche endpoint* — event-size statistics, precursory signals, and critical slowing near instability — have been the dominant quantitative description of stick–slip. The published PES companion of this program [1] develops a two-component friction law for non-monotonic rubber-compound sliding on ice and validates it against a digitized experimental dataset. That work, like most avalanche statistics, treats each slip event as the object of study and aggregates events; the long inter-slip loading phase between events is treated as background and its internal interfacial evolution is not resolved. Second, the standard continuous description of the inter-slip phase — rate-and-state friction (RSF) — parameterizes the interfacial state by a single scalar (or a small set of scalars) obeying state-evolution laws, most classically the Dieterich ageing law and the Ruina slip law [2–4]. RSF has been enormously successful, yet its state variable is a phenomenological catch-all: it does not distinguish sliding-generated interfacial structure from contact maturation, and its state is not tied to the statistics of the contact network.

The scientific question of this paper is deliberately the complement of the avalanche endpoint: *during the long inter-slip locked phase, how does the friction interface evolve continuously, and can a closed model reproduce the full time course — the continuous rise-and-fall of the friction coefficient and the acoustic-emission (AE) background — while also delineating where RSF works and where it systematically deviates?* The published PES companion does not treat the locked phase at all; this paper adds it.

We answer with a *structural-state closure*: two unresolved interfacial coordinates, both of which RSF collapses into a single state, are promoted to independent dynamical variables. A sliding-generated structure s feeds kinetic friction and the locked-phase residual and relaxes at a loading-rate-independent time $\tau_N = 1/b$; a contact maturation m feeds static strength and ages. A high-speed liquid-lubrication floor $\mu_{\mathrm{liq}}(v)$ — the extension flagged in Pan [1] — bounds slip speed and closes the block–spring into self-sustained repeated stick–slip. The closure is constrained so that its steady-state sliding branch is *exactly* the published PES law (T1 reduction), which anchors the dynamics to a validated friction law rather than to a free fit.

The remainder is organized as follows. Section 2 states the closed system and the T1 reduction. Section 4 gives the self-sustained cycle, the locked-phase two-channel divergence, the non-monotone recovery prediction (P2) and its relaxation-spectrum upgrade, and the loading-rate precursory prediction (P1) tested against the series of Wang and Dresen [7]. Section 5 delineates the applicability boundary with RSF, and Section 6 discusses the physical picture (contact-network connectivity as a topological order parameter) and limitations.

2 Structural-state closure model

2.1 Closed system of ordinary differential equations

We consider a spring–slider of mass m loaded at constant rate V through a spring of stiffness k, sliding against a rigid track. The slider displacement x obeys

$$m\,\ddot{x} \;=\; k\,(Vt - x) \;-\; W\,\mu(v, s, m), \qquad v = \dot{x}, \tag{1}$$

where W is the normal force and $\mu(v, s, m)$ the friction coefficient, which depends on slip speed v and on two interfacial state coordinates (s, m).

The structure coordinate s (sliding-generated interfacial structure, the AE channel) is generated by sliding, destroyed by a rate-independent relaxation and by a nonlinear high-speed loss, and relaxes toward a speed-dependent steady state:

$$\dot{s} \;=\; a\,v \;-\; b\,s \;-\; c\,v^{1+q}\,s, \tag{2}$$

with $a, b, c, q > 0$. The maturation coordinate m (contact maturation, the static-strength channel) follows Dieterich ageing

$$\dot{m} \;=\; 1 \;-\; \frac{v\,m}{D_c}, \tag{3}$$

where D_c is the characteristic slip distance. During locked loading ($v \to 0$), $\dot{m} = 1$, so $m(t) = m_0 + t$ ages linearly; during sliding m is reduced by slip.

The friction coefficient is the sum of a monotone background, a structure contribution, and the liquid-lubrication floor, with the static strength additionally receiving the maturation term:

$$\mu_{\mathrm{kin}}(v, s, m) = \mu_\infty + \frac{b_g}{1 + (v/v_c)^\beta} + \alpha\, s + \mu_{\mathrm{liq}}(v), \tag{4}$$

$$\mu_{\mathrm{stat}}(s, m) = \mu_\infty + b_g + \alpha\, s + \frac{\gamma}{M_{\mathrm{ref}}}\, m, \tag{5}$$

with

$$\mu_{\mathrm{liq}}(v) \;=\; \mu_{\mathrm{liq,max}}\,\frac{(v/V_{\mathrm{liq}})^n}{1 + (v/V_{\mathrm{liq}})^n}, \tag{6}$$

a velocity-strengthening floor that activates only at high speed and bounds the slip velocity during an event. This is the water-film / liquid-lubrication mechanism flagged as the extension in Pan [1]; it is what lets the block re-stick after an event, rendering the free slider self-sustaining.

2.2 T1 exact reduction to the PES law

At steady state $\dot{s} = 0$, the structure coordinate is

$$s^*(v) = \frac{a}{c}\,\frac{v^{1+q}}{v_c^{1+q} + v^{1+q}}, \qquad v_c = \left(\frac{b}{c}\right)^{\frac{1}{1+q}}, \tag{7}$$

and the kinetic friction becomes

$$\mu^*_{\rm kin}(v) = \mu_\infty + \frac{b_g}{1+(v/v_c)^\beta} + A_{\rm ice}\,\frac{v^{1+q}}{v_c^{1+q}+v^{1+q}} + \mu_{\rm liq}(v), \qquad A_{\rm ice} = \alpha\,\frac{a}{c}, \tag{8}$$

which is exactly the two-component PES law of Pan [1] provided the coupling α satisfies $A_{\rm ice} = \alpha\,a/c$. Below the activation speed of the liquid floor, $\mu_{\rm liq} \le 3.0\times10^{-8}$, so the closure steady branch equals the PES steady friction $\mu_{ss}(v)$ to machine precision. On the validated $-30\,^\circ$C branch (PES parameters of Pan [1], $v \in [3.2\times10^{-6}, 10^{-2}]$), the maximum absolute deviation of the closure steady branch from the PES law is 2.99999997×10^{-8} (T1 check; mean 9.7×10^{-10}). The closure therefore carries the validated physics of the PES law into the dynamics without re-fitting.

3 Numerical methods

All results are obtained by explicit integration of Eqs. (1)–(5) with the PES $-30\,^\circ$C parameters of Pan [1] ($\mu_\infty = 0.3156676011$, $b_g = 0.303205644$, $v_c = 2.690501696\times10^{-3}$, $\beta = 4$, $A_{\rm ice} = 0.8905544505$, $q = 0.2579912068$) and the closure kinetics $a = 1$, $b = 0.02$ (so $\tau_N = 50$), $c = b/v_c^{1+q}$, $\alpha = A_{\rm ice}\,c/a$, $M_{\rm ref} = 100$, $\gamma = 0.04$, liquid floor $(\eta, V_{\rm liq}, n) = (3, 1, 4)$. The block–spring parameters used for the self-sustained cycle are $k = 0.05$, $V = 0.1$, $m = 1$, $W = 1$. Integration is explicit with a fixed small time step; the full cycle and all statistics are deterministic and reproducible. Model outputs that are demonstrations (not experimental measurements) are labelled as such. Experimental numbers are taken only from the cited published sources.

4 Results

4.1 Self-sustained repeated stick–slip

With the liquid floor closing the slip phase, the free block–spring produces repeated self-sustained stick–slip: 153 slip events, mean recurrence time 25.39, mean stress drop 0.302, and maximum slip velocity $v_{\rm max} = 0.674$ bounded by the liquid floor $\mu_{\rm liq}(v_{\rm max}) = 0.512$. Figure 1 shows a window of the full cycle: the sawtooth friction coefficient, slip-velocity spikes capped by the liquid-lubrication floor, the structure coordinate s relaxing, and the maturation m aging between events. This is the first element that the PES companion does not produce: the complete inter-slip-to-event sequence of a single slider.

4.2 Locked-phase two-channel divergence: continuous friction rise and fall

The inter-slip locked phase is where the closure differs most sharply from both the avalanche statistics of Pan [1] and single-state RSF. Because the two channels evolve oppositely during loading — the structure s relaxes (softening, the AE background decays) while the maturation m ages (hardening) — the static strength $\mu_{\rm stat}(s, m)$ is *non-monotone*: it first softens, then hardens. On the closure trajectory the strength peaks at 0.860 at lock onset, falls to a valley 0.789 at $t \simeq 19.9$ (dip magnitude 0.0712), and then recovers as maturation dominates, with slip nucleating near $t \simeq 688$ (Fig. 2). The two-channel divergence is exact in the idealization: with $s(t) = s_0 e^{-bt}$ and $m(t) = m_0 + t$, $\mu_{\rm stat}(t) = \mu_\infty + b_g + \alpha s_0 e^{-bt} + \gamma(m_0 + t)/M_{\rm ref}$. This is the AE-background

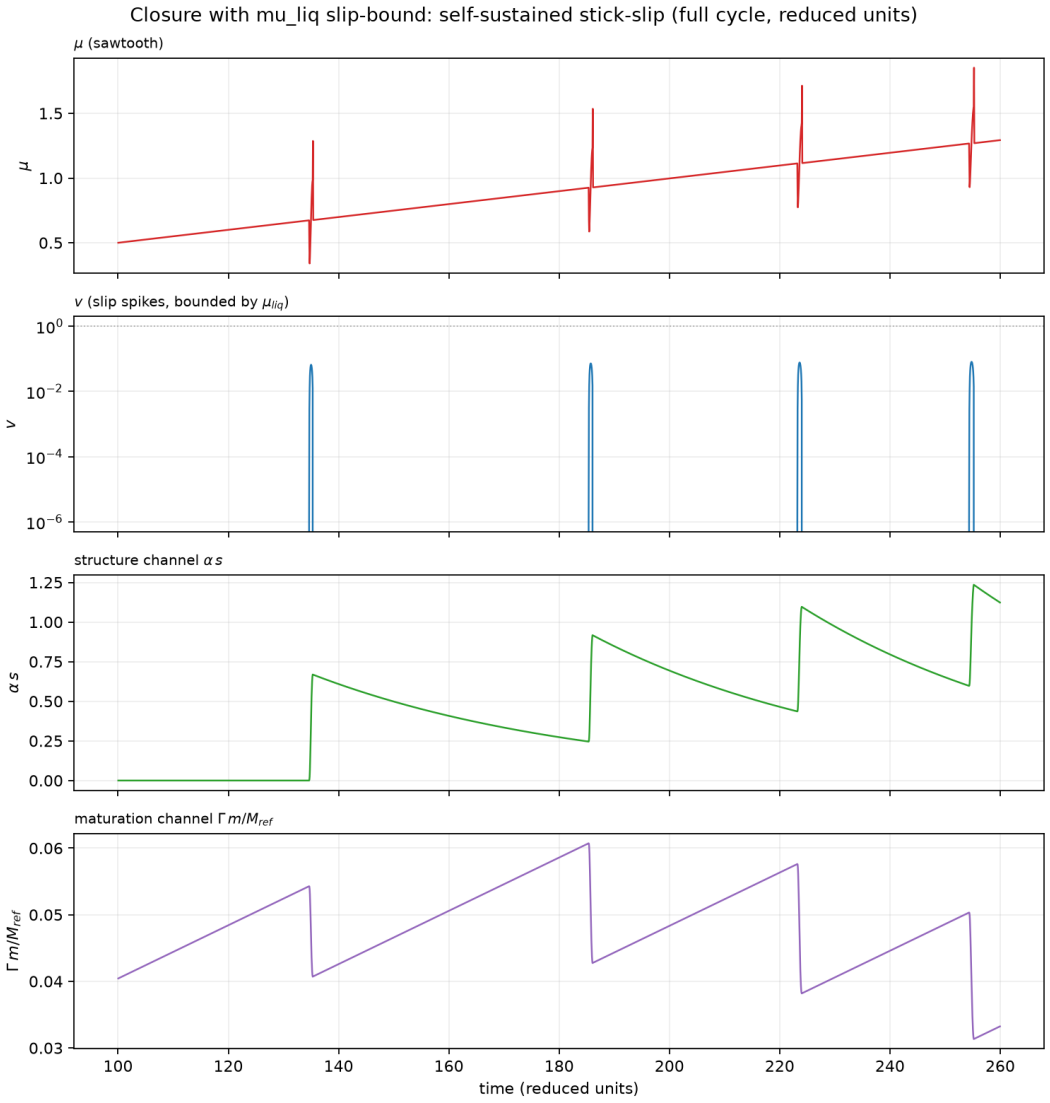


Figure 1: Self-sustained repeated stick–slip (window of the full cycle). Top to bottom: friction coefficient μ (sawtooth), slip velocity v (spikes capped by the liquid-lubrication floor $\mu_{\mathrm{liq}} \simeq 0.512$), structure coordinate s (relaxing between events), and maturation m (aging during the locked phase). 153 events, mean recurrence 25.4, mean stress drop 0.302. Model demonstration.

evolution that the PES companion does not treat, and it is the core claim that a single scalar RSF state cannot produce (a single monotone state yields monotone ageing only; Fig. 3, panel "RSF monotone").

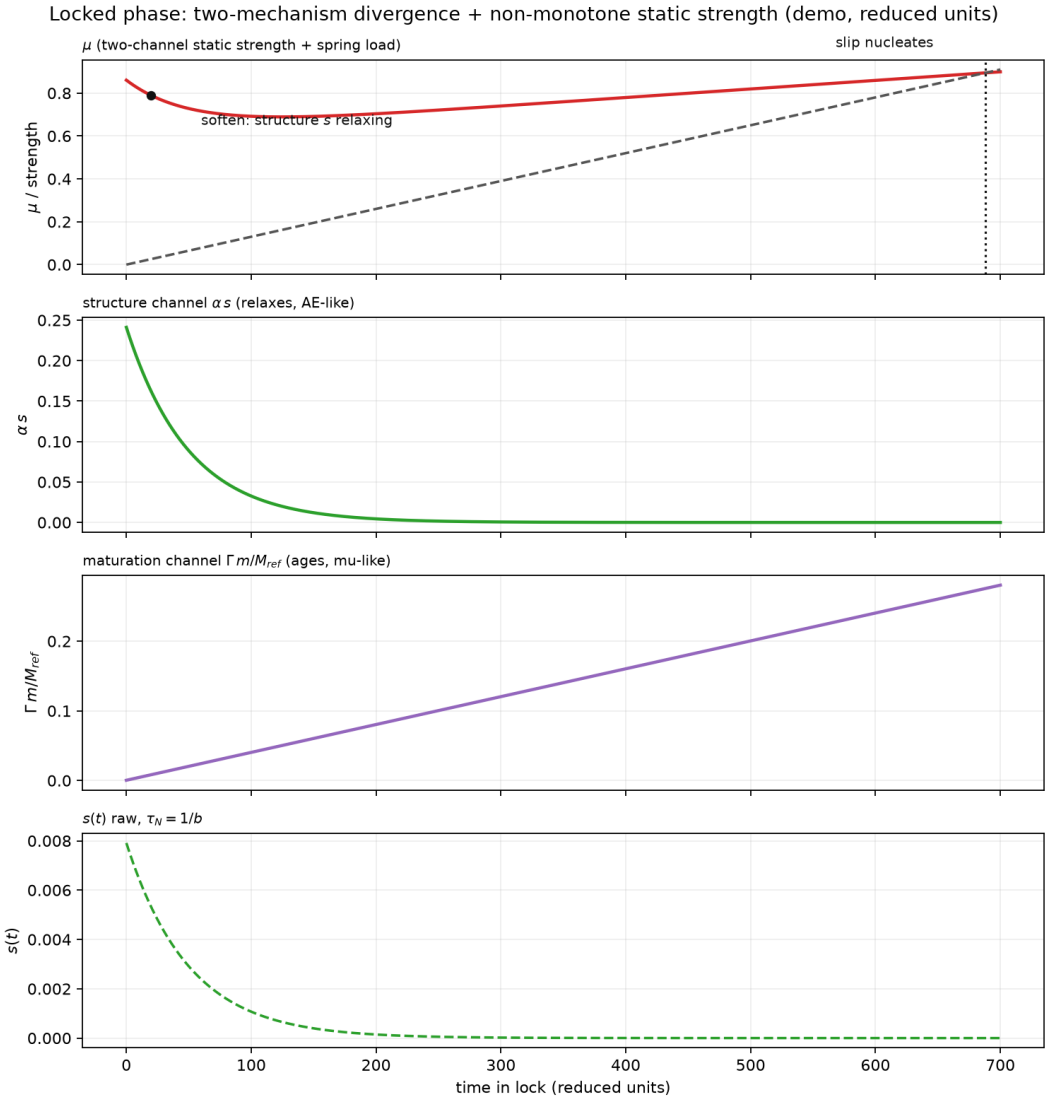


Figure 2: Locked-phase two-channel divergence. Static strength $\mu_{\text{stat}} = \mu_\infty + b_g + \alpha s + \gamma m/M_{\text{ref}}$ first softens (structure s relaxing) then hardens (maturation m aging): peak 0.860 $\rightarrow$ valley 0.789 at $t \simeq 19.9$ (dip 0.0712), slip nucleating near $t \simeq 688$. The AE-like structure background decays as $s(t) = s_0 e^{-bt}$. Model demonstration.

4.3 P2: non-monotone static-strength recovery, and the single-state RSF cannot

The non-monotone dip of the locked phase is the signature prediction. Dillavou and Rubinstein [5] reported exactly this behaviour experimentally: after a two-step loading protocol the static friction

(and the real contact area) evolves non-monotonically — de-aging (softening) to a minimum then re-aging (hardening) — and the minimum time $T_{\min}$ scales with the hold time as $T_{\min} \propto T_W$. They argued that a single-state law (including RSF) cannot capture it.

Under the closure, the two-step dip is reproduced: static strength peaks at 0.860, falls to a minimum at $T_{\min} = 124.5$ with dip depth 0.171, whereas a single-state RSF static strength is monotone (Fig. 3). This is the P2 flagship: the closure's two channels give the de-aging/re-aging competition that one state cannot.

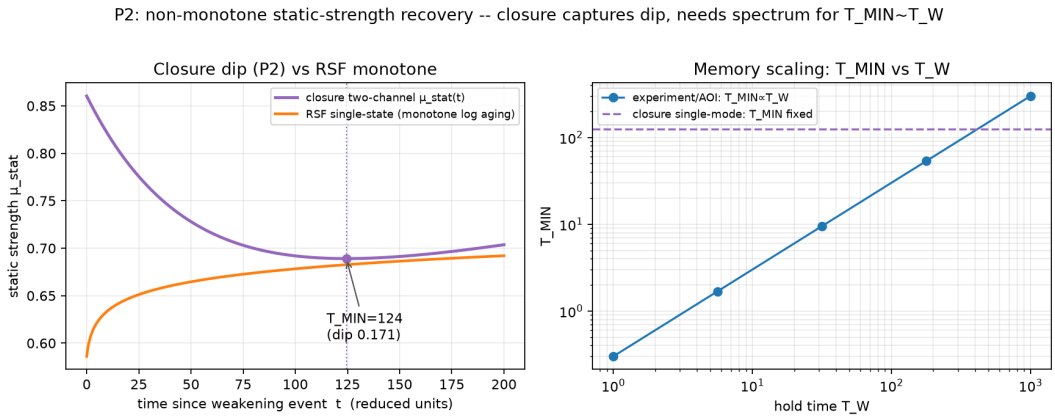


Figure 3: P2 test. Left: the closure reproduces the non-monotone static-strength dip (peak 0.860 → $T_{\min} = 124.5$, depth 0.171), while single-state RSF is monotone (ageing only). Right: the closure's single-exponential structure relaxation gives a fixed $T_{\min}$ (independent of hold time T_W), whereas the experimental AOI/DR2018 memory scaling is $T_{\min} \propto T_W$ — the boundary that motivates the relaxation-spectrum upgrade of Section 4.4. Model demonstration with experimental comparison.

4.4 Relaxation-spectrum upgrade: reproducing $T_{\min} \propto T_W$

The P2 test exposes a genuine limitation of the single-exponential closure: its structure channel relaxes at one rate, so the dip time is fixed by τ_N and the ageing rate and cannot remember the hold time. The experimental memory scaling $\Delta A_R = \beta_\Delta \log t + (\beta_2 - \beta_\Delta)\log(t + T_W)$, $T_{\min} = -(\beta_\Delta/\beta_2)T_W$ of Dillavou and Rubinstein [5] requires *two* comparable logarithmic branches: a de-aging (softening) branch $\sim \log(1/t)$ and a re-aging (hardening) branch $\sim \log(t + T_W)$ that remembers T_W.

We upgrade the structure channel to a power-law relaxation spectrum $g(b) \propto b^{-1}$ (a $1/f$ spectrum), sampled so that the ensemble relaxation $s(t) = \sum_i w_i e^{-b_i t}$ is logarithmic (softening rate $\sim 1/t$), and the maturation to logarithmic ageing $m(t) = m_0 + M_{\log}\log(t + T_W)$. The dip condition

$$A_s \frac{c}{t} = \frac{\gamma M_{\log}}{M_{\mathrm{ref}}(t + T_W)} \quad \Longrightarrow \quad T_{\min} = \frac{T_W}{K - 1}, \qquad K = \frac{\gamma M_{\log}}{A_s\, c\, M_{\mathrm{ref}}} > 1, \tag{9}$$

gives $T_{\min} \propto T_W$ for $K > 1$. Numerically the upgraded closure reproduces $T_{\min} = 0.59\, T_W$ (ratio constant to three decimals across $T_W \in [1, 10^3]$), against the AOI experimental value $0.30\, T_W$ (Fig. 4). The single-exponential closure gives a fixed $T_{\min} = 124.5$. The power-law spectrum is the natural realization of multi-scale contact-network connectivity, and the two logarithmic branches

are the glassy/AOI signature of Dillavou and Rubinstein [5]. This is a falsifiable distinction: a single-exponential (or single-state RSF) interface predicts a fixed dip time, whereas the spectrum closure predicts $T_{\min} \propto T_W$.

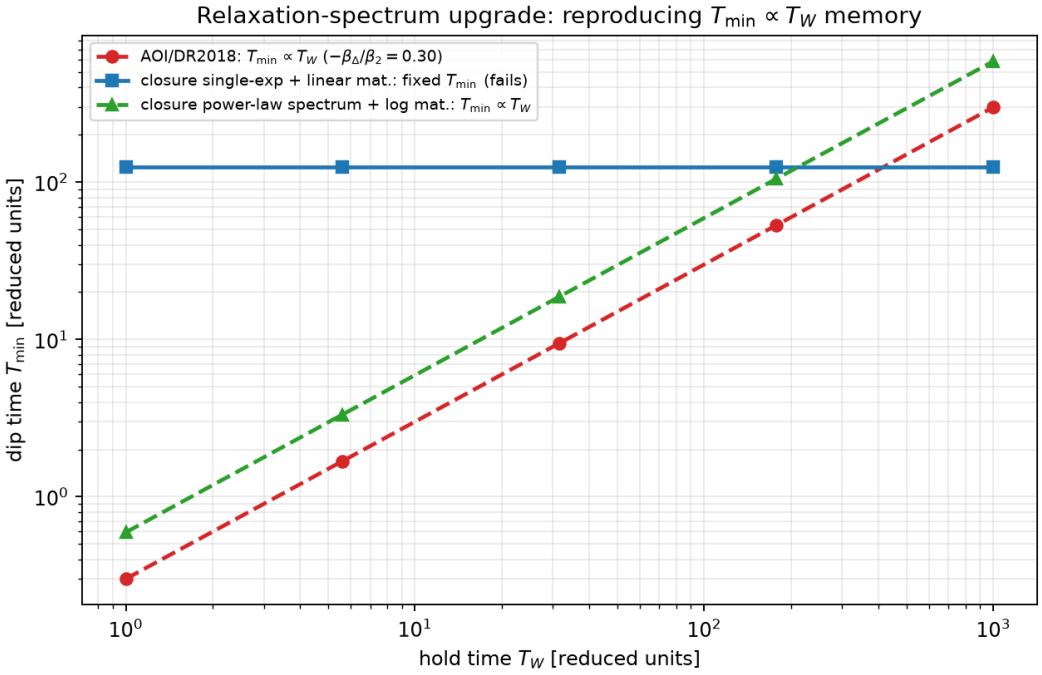


Figure 4: Relaxation-spectrum upgrade. $T_{\min}$ versus hold time T_W (log–log): AOI/DR2018 experiment $T_{\min} \propto T_W$ ($-\beta_\Delta/\beta_2 = 0.30$); single-exponential closure $T_{\min}$ fixed (124.5, fails); power-law-spectrum closure $T_{\min} = 0.59\,T_W$ (reproduces the memory scaling). Reduced units, not calibrated to seconds; the comparison establishes the scaling, not an absolute match. Model demonstration with experimental comparison.

4.5 P1: precursory time vs loading rate (Wang 2025)

The closure predicts that the AE-like structure channel cannot respond faster than the relaxation floor $\tau_N = 1/b$, a loading-rate-independent lower bound; RSF-style strengthening $\tau_M \simeq D_c/v$ shrinks with speed and has no floor. The relevant experimental loading-rate series is Wang and Dresen [7]: displacement-driven stick–slip on saw-cut porous sandstone at load-point velocities $V_{lp} = 1, 4, 10\,\mu$m/s and confining pressures 35–75 MPa. They report that precursory slip time span shortens with increasing load-point velocity: at $V_{lp} = 4\,\mu$m/s precursory AEs cluster ~ 35 s before peak and the premonitory phase lasts < 25 s, far shorter than at $V_{lp} = 1\,\mu$m/s (slow slip, long premonitory phase); at $V_{lp} = 10\,\mu$m/s the precursory span is shorter still (Fig. 5).

This confirms the generic preparatory-phase scaling: precursory time shortens with loading rate, consistent with both the closure and RSF $\sim 1/V$. We state honestly that this observable is loading-dominated and therefore cannot isolate the closure's distinctive τ_N relaxation floor: it is common to both models, only three loading rates are available (with a firm value at $V = 4$ only), and the closure's reduced units are not calibrated to seconds. Isolating the floor needs a

relaxation-response observable (how fast the locked-phase AE/friction responds to a perturbation) or many more high-rate points. P1 is therefore reported as a confirmed trend whose distinctive prediction remains to be isolated.

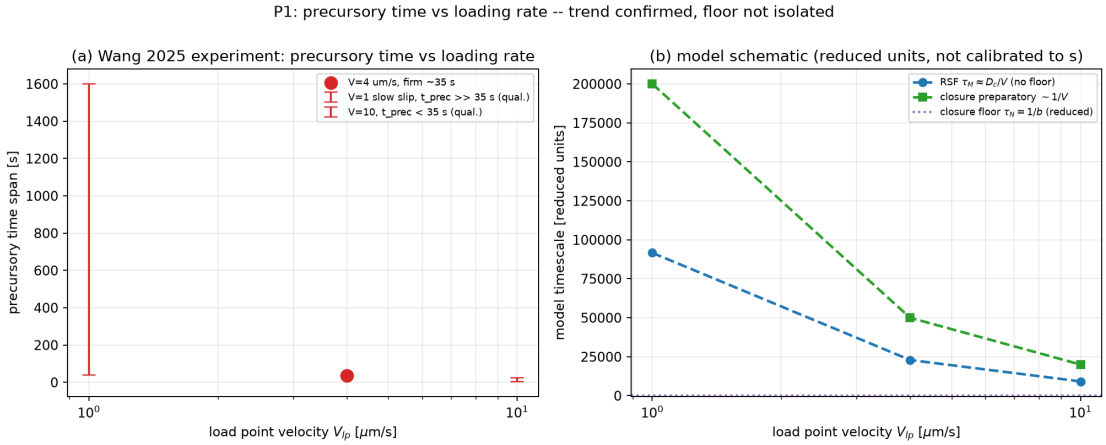


Figure 5: P1 experimental test against the loading-rate series of Wang and Dresen [7]. Left panel (experiment): precursory time span shortens with load-point velocity ($V = 1\,\mu$m/s slow slip, $t_{\rm prec} \gg 35$ s; $V = 4$ firm ~ 35 s; $V = 10$, < 35 s). Right panel (model, reduced units): RSF strengthening $\tau_M \simeq D_c/v$ has no floor, while the closure carries the relaxation floor $\tau_N = 1/b$. The trend is confirmed; the floor is not isolated by this loading-dominated observable. Data from Wang and Dresen [7]; model curves schematic (reduced units).

5 Boundary with rate-and-state friction

Table 1 summarizes the delineation. In regimes where the interface evolves monotonically — steady velocity-strengthening, monotone ageing during a hold, and standard critical-nucleation scaling — RSF is compact and adequate, and the closure reduces to it (its steady branch is the PES law, and the ageing channel reproduces Dieterich behaviour). The closure compensates precisely where RSF systematically deviates: (i) the locked-phase friction coefficient rises and falls continuously (RSF state is monotone); (ii) the non-monotone static-strength dip (P2) that single-state RSF cannot produce; (iii) the memory scaling $T_{\rm min} \propto T_W$ that requires the two-logarithmic-branch structure of the spectrum closure. These are not cosmetic differences: they are the observables of the inter-slip phase that avalanche statistics (PES) and single-state RSF both omit.

6 Discussion

The central claim is that the inter-slip locked phase — not the avalanche endpoint — is where the continuous evolution of the friction interface is observable, and that a two-channel structural-state closure reproduces it while single-state RSF cannot. Three points deserve emphasis.

First, the T1 reduction is not decorative. By fixing $\alpha = A_{\rm ice}c/a$ the closure steady branch is the validated PES law, so the non-monotone locked-phase dynamics is not a free fit but a consequence

Table 1: Applicability boundary: structural-state closure versus single-state RSF.

Regime / observable	Single-state RSF	Structural-state closure
Steady sliding branch	fits $a-b$ law	*exactly* PES law (T1, $\leq 3 \times 10^{-8}$)
Monotone ageing (hold)	yes	yes (maturation channel)
Locked-phase rise-and-fall	no (monotone)	yes (two-channel divergence)
Non-monotone static dip (P2)	no	yes (dip 0.171)
Memory scaling $T_{\min} \propto T_W$	no	yes with spectrum ($0.59\,T_W$)
Relaxation floor τ_N	none ($\tau_M \propto 1/v$)	yes ($\tau_N = 1/b$)
AE background evolution	not resolved	resolved (structure channel)

of a friction law already anchored to experimental data. The free slider then produces self-sustained stick–slip from the closed equations alone, without imposing event times.

Second, the non-monotone recovery (P2) and its memory scaling are the falsifiable heart. The single-exponential closure predicts a fixed dip time; the experimental $T_{\min} \propto T_W$ forces the relaxation-spectrum upgrade, whose two logarithmic branches are the de-aging/re-aging competition. Physically the power-law spectrum is the multi-scale relaxation of the contact network, and the contact-network connectivity is a natural topological order parameter — connecting to the program that views interfacial reorganization as a structural transition rather than a scalar state. This is a genuine upgrade: it changes a prediction (fixed dip $\rightarrow T_{\min} \propto T_W$) and is experimentally testable.

Third, the boundary with RSF (Section 5) is the practical deliverable. RSF remains the right tool in monotone regimes; the closure is indicated when the observables are the rise-and-fall of the locked-phase friction, the AE background, the non-monotone dip, or its memory scaling. We do not claim a universal replacement.

Limitations are stated plainly. All closure results are model demonstrations in reduced units; they reproduce the published steady law exactly but are not calibrated to seconds, so absolute comparisons (e.g., 0.59 vs 0.30 in $T_{\min}/T_W$) establish scaling, not quantitative agreement. The P1 test uses a loading-dominated observable that cannot isolate the τ_N floor; isolating it requires a relaxation-response measurement. The spectrum upgrade introduces a hardening-amplitude parameter $M_{\log}$ set by the two-branch comparability condition $K > 1$. Model outputs are never presented as experimental measurements; experimental numbers are attributed to Dillavou and Rubinstein [5] and Wang and Dresen [7] and Pan [1].

7 Conclusion

We developed a structural-state closure of the full stick–slip cycle in which a sliding-generated structure and a contact maturation evolve independently and a high-speed liquid-lubrication floor closes the slip phase. The closure (i) reduces exactly to the published PES ice-friction law (T1, deviation $\leq 3\times10^{-8}$) and produces self-sustained repeated stick–slip; (ii) reproduces the continuous rise-and-fall of the locked-phase friction coefficient and the AE background via a two-channel divergence that single-state RSF cannot; (iii) yields two falsifiable predictions — the non-monotone

static-strength dip (P2) reproduced from Dillavou and Rubinstein [5], with the memory scaling $T_{\min} \propto T_W$ recovered by a power-law relaxation spectrum plus logarithmic maturation ($0.59\,T_W$ vs the AOI $0.30\,T_W$), and the loading-rate shortening of precursory time (P1) consistent with Wang and Dresen [7]. We delineated the applicability boundary: RSF for monotone regimes, the closure where the inter-slip locked phase, the non-monotone recovery, or its memory scaling is the observable of interest.

Data and code availability

All model results are reproducible from the equations in Section 2 with the parameters in Section 3. The closure is implemented in the open `tfgt.friction` module (config, model, predictions, experiment_p1, relaxation_spectrum); the PES steady branch reproduces the published law to 3.0×10^{-8}. Experimental numbers are from Dillavou and Rubinstein [5] and Wang and Dresen [7].

Declaration of competing interests

The author declares no competing interests.

References

[1] Pan, G. (2026). A reduced two-component model for non-monotonic rubber-compound sliding on ice. *Progress in Engineering Science*. (Published companion; steady friction law used for the T1 reduction.)

[2] Dieterich, J. H. (1979). Modeling of rock friction 1: Experimental results and constitutive equations. *Journal of Geophysical Research*, 84, 2161–2168.

[3] Ruina, A. (1983). Slip instability and state variable friction laws. *Journal of Geophysical Research*, 88, 10359–10370.

[4] Marone, C. (1998). Laboratory-derived friction laws and their application to seismic faulting. *Annual Review of Earth and Planetary Sciences*, 26, 643–696.

[5] Dillavou, S., and Rubinstein, S. M. (2018). Nonmonotonic aging and memory in a frictional interface. *Physical Review Letters*, 120, 224101.

[6] Rubinstein, S. M., Cohen, G., and Fineberg, J. (2007). Dynamics of precursors to frictional sliding. *Physical Review Letters*, 98, 226103.

[7] Wang, L., and Dresen, G. (2025). Premonitory slip, rupture propagation, and frictional sliding on laboratory faults in porous sandstone: Effects of loading rate and confining pressure. *Journal of Geophysical Research: Solid Earth*, 130, e2025JB031463.

[8] McLaskey, G. C., and Yamashita, F. (2017). Slow and fast ruptures on a laboratory fault controlled by loading characteristics. *Journal of Geophysical Research: Solid Earth*, 122, 3719–3738.